

Asymptotic analysis of quasielastic neutron scattering data from human acetylcholinesterase reveals subtle dynamical changes upon ligand binding

Cite as: J. Chem. Phys. 150, 161104 (2019); <https://doi.org/10.1063/1.5094625>

Submitted: 04 March 2019 . Accepted: 09 April 2019 . Published Online: 30 April 2019

Melek Saouessi , Judith Peters , and Gerald R. Kneller 



View Online



Export Citation



CrossMark

The Journal
of Chemical Physics

2018 EDITORS' CHOICE

READ NOW!

AIP
Publishing

Asymptotic analysis of quasielastic neutron scattering data from human acetylcholinesterase reveals subtle dynamical changes upon ligand binding

Cite as: J. Chem. Phys. 150, 161104 (2019); doi: 10.1063/1.5094625

Submitted: 4 March 2019 • Accepted: 9 April 2019 •

Published Online: 30 April 2019



View Online



Export Citation



CrossMark

Melek Saouessi,^{1,2}  Judith Peters,^{3,4}  and Gerald R. Kneller^{1,2,a)} 

AFFILIATIONS

¹Centre de Biophysique Moléculaire, CNRS and Université d'Orléans, Rue Charles Sadron, 45071 Orléans, France

²Synchrotron Soleil, L'Orme de Merisiers, 91192 Gif-sur-Yvette, France

³Institut Laue Langevin, 71 Avenue des Martyrs, 38042 Grenoble Cedex 9, France

⁴Université Grenoble Alpes, CNRS, Laboratoire Interdisciplinaire de Physique, F-38000 Grenoble, France

^{a)}E-mail: gerald.kneller@cnrs.fr

ABSTRACT

In this paper, we show that subtle changes in the internal dynamics of human acetylcholinesterase upon ligand binding can be extracted from quasielastic neutron scattering data by employing a nonexponential relaxation model for the intermediate scattering function. The relaxation is here described by a stretched Mittag-Leffler function, which exhibits slow power law decay for long times. Our analysis reveals that binding of a Huperzine A ligand increases the atomic motional amplitudes of the enzyme and slightly slows down its internal diffusive motions. This result is interpreted within an energy landscape picture for the motion of the hydrogen atoms.

Published under license by AIP Publishing. <https://doi.org/10.1063/1.5094625>

Thermal incoherent neutron scattering is a powerful tool to study the dynamical properties of condensed soft matter systems at nanometric length scales and time scales between subpicoseconds and several nanoseconds.¹ Due to the dominance of incoherent scattering from hydrogen atoms, neutron scattering gives a molecule-averaged view of the dynamics of hydrogen-rich macromolecules, such as (bio)polymers. For an overview, the reader may consult Refs. 2 and 3. A particularly interesting field of application is here the study of functional enzyme dynamics upon ligand binding.^{4,5} In the following, we will be concerned with analyzing quasielastic neutron scattering (QENS) spectra from hydrated powders of human acetylcholinesterase (hAChE) with and without a noncovalently bound Huperzine A (HupA) ligand. The data have been collected on the IN6 spectrometer at the Institut Laue-Langevin in Grenoble. The experimental details have been published recently, and a corresponding previous data analysis did not reveal systematic dynamical changes upon binding of the HupA ligand.^{6–8} The term “dynamical changes” concerns here the change of motional amplitudes, which are probed by elastic scattering, and the change of the

diffusional/relaxational dynamics, which is probed by quasielastic scattering.

Due to the dominant incoherent scattering of the hydrogen atoms, the differential scattering cross section of the hydrogen-rich hAChE powders, i.e., the measured intensities, may be approximated by

$$\frac{d^2\sigma}{d\Omega d\omega} \approx |b_{\text{H,inc}}|^2 \frac{|\mathbf{k}|}{|\mathbf{k}_0|} S(\mathbf{q}, \omega), \quad (1)$$

where $b_{\text{H,inc}}$ is the incoherent scattering length of hydrogen and $S(\mathbf{q}, \omega)$ is the dynamic structure factor. The latter is the quantity of interest in neutron spectroscopy and its arguments $\mathbf{q} = \mathbf{k}_0 - \mathbf{k}$ and ω are the momentum and energy transfers from the neutrons to the scattering hydrogen atoms in units of \hbar . The dynamic structure factor is the time Fourier transform of the intermediate scattering function, $F(\mathbf{q}, t)$,

$$S(\mathbf{q}, \omega) = \frac{1}{2\pi} \int_{-\infty}^{+\infty} dt e^{-i\omega t} F(\mathbf{q}, t), \quad (2)$$

which is a quantum time correlation function. In protein powder samples, where rigid-body motions of whole protein molecules are suppressed, the QENS spectrum has an elastic component and $F(\mathbf{q}, t)$ has the generic form

$$F(\mathbf{q}, t) = EISF(\mathbf{q}) + (1 - EISF(\mathbf{q}))\phi(\mathbf{q}, t), \quad (3)$$

where $EISF(\mathbf{q})$ stands for “elastic incoherent structure factor” and $\phi(\mathbf{q}, t)$ is a relaxation function fulfilling $\phi(\mathbf{q}, 0) = 1$ and $\lim_{t \rightarrow \infty} \phi(\mathbf{q}, t) = 0$. Defining $\hat{\rho}_\alpha(\mathbf{q}, t) = \exp(i\mathbf{q} \cdot \hat{\mathbf{r}}_\alpha(t))$ to be the Fourier transformed single particle density of hydrogen atom α at position $\hat{\mathbf{r}}_\alpha(t)$, we have

$$EISF(\mathbf{q}) = \frac{1}{N} \sum_{\alpha \in H} |\langle \hat{\rho}_\alpha(\mathbf{q}) \rangle|^2, \quad (4)$$

$$\phi(\mathbf{q}, t) = \frac{1}{N} \sum_{\alpha \in H} \frac{\langle \delta \hat{\rho}_\alpha^\dagger(\mathbf{q}, 0) \delta \hat{\rho}_\alpha(\mathbf{q}, t) \rangle}{\langle \delta \hat{\rho}_\alpha^\dagger(\mathbf{q}, 0) \delta \hat{\rho}_\alpha(\mathbf{q}, 0) \rangle}, \quad (5)$$

where $\delta \hat{\rho}_\alpha(\mathbf{q}, t) = \hat{\rho}_\alpha(\mathbf{q}, t) - \langle \hat{\rho}_\alpha(\mathbf{q}, 0) \rangle$. The symbol $\langle \dots \rangle$ indicates a quantum thermal average and $\phi(\mathbf{q}, t)$ is a quantum time correlation function fulfilling

$$\phi(\mathbf{q}, t) = \phi(-\mathbf{q}, -t + i\beta\hbar), \quad (6)$$

with $\beta = (k_B T)^{-1}$. For the following considerations, we introduce the symmetrized relaxation function

$$\phi^{(+)}(t) = \frac{\phi(t + i\beta\hbar/2)}{\phi(i\beta\hbar/2)}, \quad (7)$$

where the \mathbf{q} -dependence can be omitted due to the fact that $\phi(-\mathbf{q}, t) = \phi(\mathbf{q}, t)$ in powder samples. By construction, $\phi^{(+)}(\mathbf{q}, 0) = 1$, and we write with (3),

$$F^{(+)}(t) = EISF + (1 - EISF)\phi^{(+)}(t). \quad (8)$$

The overwhelming part of QENS studies is and has been interpreted by using the classical limit of Van Hove’s theory,⁹ using classical diffusion models to describe the dynamics of the hydrogen atoms. In this case, $F^{(+)}(t)$ is replaced by the classical limit of the intermediate scattering function, $F_{cl}(t) = \lim_{\hbar \rightarrow 0} F(t)$. Besides the fact that recoil effects are neglected, the use of such models becomes to some extent meaningless for complex molecular systems, such as proteins, where each atom participates in a large spectrum of motion types with an associated large spectrum of time scales.¹⁰ Based on these insights, we propose a corresponding analysis of QENS data using a simple minimal model for the intermediate scattering function. The relaxation function $\phi^{(+)}(t)$ is here represented by a stretched Mittag-Leffler (ML) function

$$\phi^{(+)}(t) = E_\alpha(-[t/\tau]^\alpha) \quad (0 < \alpha \leq 1, \tau > 0), \quad (9)$$

which behaves for large arguments as $\phi^{(+)}(t) \sim \sum_{k=1}^M (-1)^{k+1} (t/\tau)^{-k\alpha} / \Gamma(1 - \alpha k)$. $M\alpha > 1$ assures that all terms with a slow power law decay $\propto t^{-\gamma}$, with $0 < \gamma < 1$, are included. The Mittag-Leffler function has the series representation¹¹ $E_\alpha(z) = \sum_{n=0}^{\infty} z^n / \Gamma(1 + \alpha n)$ and can be considered as a generalization of the exponential function, which is retrieved for $\alpha = 1$. Our choice for the relaxation function is motivated by earlier work on protein dynamics studied by

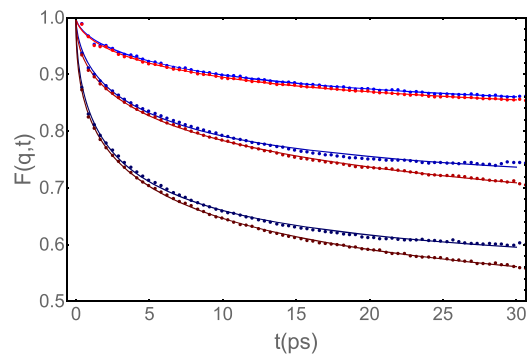


FIG. 1. $F(q, t)$ obtained from the resolution-deconvolved QENS spectra (points) and corresponding model fits (solid lines) for $q = 0.5, 0.9, 1.5 \text{ \AA}^{-1}$ from top to bottom. Blue and red correspond, respectively, to free and HupA-inhibited hAChE

neutron scattering, where it describes the relaxation of the position autocorrelation function.¹²

Figure 1 displays the intermediate scattering function obtained from the resolution-deconvolved QENS spectra for three different q -values and the corresponding fits of Expression (8) with $\phi^{(+)}(t)$ according to (9). We define here $q \equiv |\mathbf{q}|$. The extraction of the intermediate scattering function from the experimental QENS spectrum is described in the supplementary material. Figure 2 shows for a selected q -value the resolution-broadened model (and by definition noise-free) symmetrized dynamic structure factor

$$S_{\text{exp}}^{(+)}(\omega) = R(\omega) * S(\omega), \quad (10)$$

where “ $*$ ” denotes a convolution integral, $S_{\text{exp}}^{(+)}(\omega) \propto \exp(-\beta\hbar\omega/2)$ $S_{\text{exp}}(\omega)$ is the symmetrized experimental dynamic structure factor¹³ which is normalized such that $F_{\text{exp}}^{(+)}(0) = 1$, and $R(\omega)$ is the resolution function. The latter has been obtained from a vanadium run and has approximately Gaussian shape, with a FWHM of $\approx 70 \text{ } \mu\text{eV}$. With (8), it follows then that

$$S(\omega) = EISF\delta(\omega) + (1 - EISF)\tilde{\phi}^{(+)}(\omega), \quad (11)$$

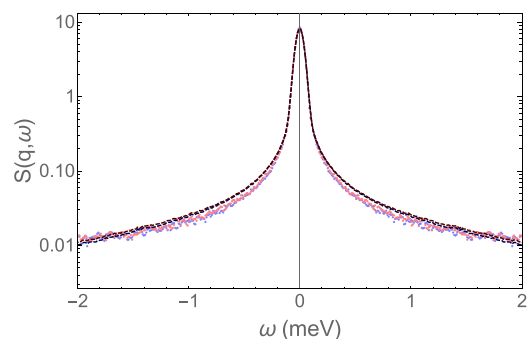


FIG. 2. Experimental QENS spectra for $q = 1 \text{ \AA}^{-1}$ (points) and corresponding convolution-broadened model fits (solid lines) in lin-log representation. Blue and red correspond, respectively, to free and HupA-inhibited hAChE.

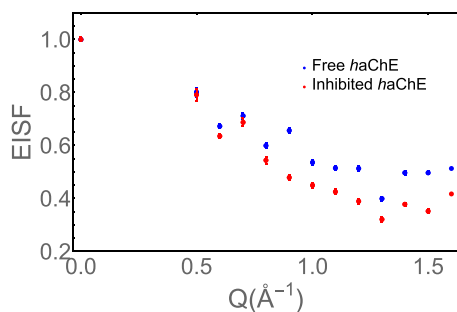


FIG. 3. EISF obtained from the fit of Expression (8), with $\phi^{(+)}(t)$ defined by Eq. (9), for free and HupA-inhibited hAChE (blue and red dots, respectively). The fits are supplemented by estimated here almost invisible error bars.

where¹⁴

$$\tilde{\phi}^{(+)}(\omega) = \frac{\sin\left(\frac{\pi\alpha}{2}\right)}{\pi|\omega|\left((\tau|\omega|)^{-\alpha} + (\tau|\omega|)^{\alpha} + 2\cos\left(\frac{\pi\alpha}{2}\right)\right)}. \quad (12)$$

The model spectra shown in Fig. 2 have been computed by discrete Fourier transform of $F_{\text{exp}}(t) = r(t)F(t)$ for the full accessible time range of IN6, which is here $t_{\text{max}} = 206$ ps, and $r(t)$ denotes the resolution window in the time domain.

Figure 3 displays the fitted EISF for free and HupA-inhibited hAChE. The results show that the EISF in the latter case is slightly smaller than its counterpart for the free variant. This reflects that the average motional amplitudes of the (hydrogen) atoms become slightly larger in presence of the HupA ligand. This is compatible with the results described in Peters *et al.*⁸ and the work by Balog *et al.*, who find by atomic detail normal mode analysis that binding of the cancer drug methotrexate softens the low-frequency/large amplitude vibrations of its target protein, dihydrofolate reductase⁵ and explain in this way earlier neutron scattering results.¹⁵ The “softening” of the low frequency modes leads, in fact, to smaller force constants for the local harmonic potential of the (hydrogen) atoms and thus to larger motional amplitudes. However, this result cannot be generalized since inverse cases are also reported in the literature. Examples can be found in Refs. 8 and 16.

While the EISF expresses the amplitudes of the atomic motions, the parameters τ and α describe their relaxation dynamics and

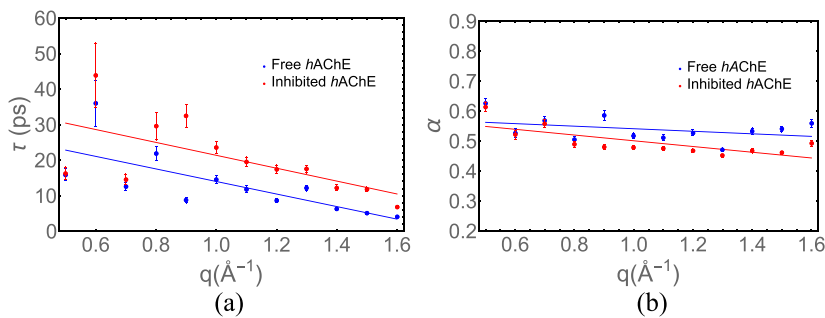


FIG. 4. Parameters α and τ for free and HupA-inhibited hAChE as a function of q (blue and red, respectively). Points correspond to fitted parameters and solid lines to linear fits. The fits are supplemented by estimated error bars.

thus truly dynamical properties of hAChE. The q -dependence of τ and α is summarized in Fig. 4. Blue and red points again represent the fitted parameters for free and HupA-inhibited hAChE, respectively, and the corresponding solid lines correspond to linear fits. One observes that both series for the τ -parameter decay with q , where the one for inhibited hAChE displays larger values as the one for the free counterpart. The decrease of τ with q , which is seen for both free and inhibited hAChE, reflects the fact that localized motions are faster than large scale motions, whereas the general increase of τ upon inhibition of hAChE indicates slower relaxation of the inhibited variant. In contrast to the scale parameter τ , the form parameter α of the relaxation function exhibits a much weaker q -dependence, where the values for the inhibited variant of hAChE are slightly smaller than those of the free one. Noting that $\alpha = 1$ corresponds to exponential relaxation, this means that the corresponding relaxation dynamics is less exponential for the inhibited variant. In order to understand the physical meaning of the α -parameter, we write the stretched Mittag-Leffler function as a continuous superposition of exponential functions,

$$E_{\alpha}(-t^{\alpha}) = \int_0^{\infty} p(\lambda) \exp(-\lambda t) d\lambda, \quad (13)$$

which expresses the dynamical heterogeneity in a system that is composed of a large number of atoms and where each atom contributes exponentially with a different relaxation constant, λ . Here both t and λ are dimensionless and

$$p(\lambda) = \frac{1}{\pi} \frac{\sin(\pi\alpha)}{\lambda(\lambda^{\alpha} + \lambda^{-\alpha} + 2\cos(\pi\alpha))} \quad (14)$$

is a normalized relaxation rate spectrum fulfilling $\int_0^{\infty} p(\lambda) d\lambda = 1$. Higher moments of $p(\lambda)$ do not exist.

The relaxation rate spectrum, $p(\lambda)$, may be related to an energy barrier spectrum by assuming that the classical Fourier transformed single particle density, $\delta\rho(\mathbf{q}, t) = \exp(i\mathbf{q} \cdot \mathbf{r}(t)) - \langle \exp(i\mathbf{q} \cdot \mathbf{r}(0)) \rangle$, diffuses in a “rough” harmonic potential. Abbreviating $x(t) \equiv \delta\rho(\mathbf{q}, t)$, we write $V(x) = V_0(x) + \delta V(x)$, where $V_0(x) = Kx^2/2$ and $\delta V(x)$ define, respectively, its smooth and rough component (see panel (a) of Fig. 5). The smooth component, $V_0(x)$, tends to bring $x \equiv \delta\rho$ to zero, while the rough component, $\delta V(x)$, hinders this process by trapping x in one of the local minima which are separated by a fixed energy barrier, ΔE . The diffusion in the smooth potential is described by an Ornstein-Uhlenbeck process, where the displacement autocorrelation function relaxes exponentially, $\langle x(t)x(0) \rangle$

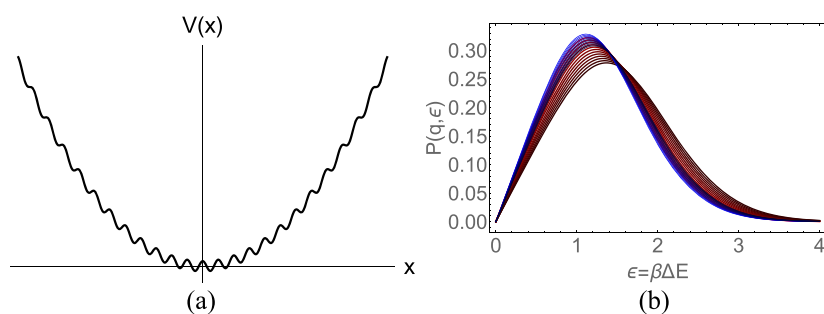


FIG. 5. (a) Sketch of a rough harmonic potential, where the minima are separated by a fixed energy barrier. (b) Model energy barrier spectrum for free and inhibited hAChE (bluish and reddish curves, respectively) from top to bottom for $q = 0.5, 0.6, \dots, 1.6/\text{\AA}$.

$= \langle x^2 \rangle \exp(-\eta_0 t)$, and where the relaxation constant and the diffusion constant are related through $D_0 = \langle x^2 \rangle \eta_0$. We use now Zwanzig's model¹⁷ for the effective diffusion in an arbitrary rough potential, $D = D_0 \exp(-[\beta \Delta E]^2)$, where $\beta = 1/(k_B T)$, which translates thus for an harmonic potential into $\eta = \eta_0 \exp(-[\beta \Delta E]^2)$ for the relaxation constant. Introducing the dimensionless energy barrier $\epsilon = \beta \Delta E$ and defining $\lambda = \eta/\eta_0$, we may write

$$\lambda = \exp(-\epsilon^2), \quad (15)$$

which leads to

$$P(\epsilon) = \frac{1}{\pi} \frac{2\epsilon \sin(\pi\alpha)}{\exp(\alpha\epsilon^2) + \exp(-\alpha\epsilon^2) + 2 \cos(\pi\alpha)} \quad (16)$$

for the distribution of the dimensionless energy barriers, ϵ . Panel (b) of Fig. 5 shows the resulting energy barrier distributions for free and inhibited hAChE (blueish and reddish curves) as a function of q , which indicate that binding of the HupA ligand shifts the energy barriers to slightly higher values and leads at the same time to a slight broadening. Ligand binding thus leads to a “roughening” of the effective potential energy surface. For both series of energy barriers, one observes a shift of the distribution to higher values with increasing q , which corresponds to looking at increasingly localized motions. This means that localized motions take place in a rougher potential than those involving the whole protein, and we note that the energy barrier shift upon fixing of the HupA ligand is

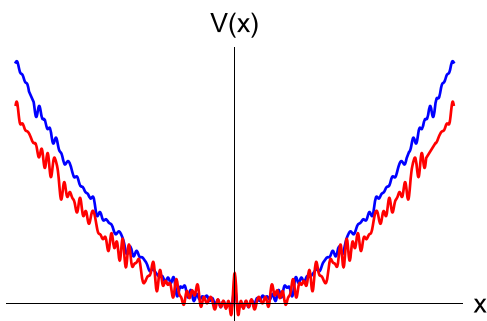


FIG. 6. Sketch of the effective energy landscapes for free and HupA inhibited hAChE (blue and red curves, respectively). More explanations are given in the text.

more pronounced. Figure 6 resumes the analysis of the QENS experiments on free and HupA-inhibited hAChE in one single sketch. The blue and the red curve correspond here, respectively, to the potential energy surface for free and inhibited hAChE, where the irregularity of the energy barriers correspond to the motional heterogeneity of the dynamics. The reduced curvature in the case of inhibited hAChE (red curve) reflects the abovementioned vibrational mode softening and explains the observed reduction of the EISF. The corresponding increased roughness of the energy surface indicates the energy barrier shift to higher values upon ligand binding.

The present work shows that a careful data analysis with an appropriate model for the intermediate scattering function, which essentially reflects its asymptotic slow power law relaxation, allows for an observation of subtle but systematic changes of the enzyme dynamics upon ligand binding. The intuitive interpretation of the results has been obtained by employing Zwanzig's physical model of diffusion in a rough quadratic potential, which translates relaxation rate spectra into energy barrier spectra. It is also worth noting that the typical barrier heights we find in our study are of the same order of magnitude as those given in Frauenfelder's paper on protein energy landscapes,¹⁸ although the latter have been obtained from flash photolysis experiments, which probe in much longer time scales than neutron scattering, and from another protein (myoglobin). This indicates the “universality” and self-similarity of protein dynamics.

We finally note that all numerical and many symbolic calculations have been performed with the Wolfram Mathematica package.¹⁹

See [supplementary material](#) for the resolution deconvolution of the experimental QENS spectra and the corresponding calculation of the intermediate scattering function.

We thank the ILL for the beam time and M. M. Koza for help on IN6. We thank P. Masson and F. Nachon for the permission to use and to reanalyze the data.

REFERENCES

- ¹M. Bée, *Quasielastic Neutron Scattering: Principles and Applications in Solid State Chemistry, Biology and Materials Science* (Adam Hilger, Bristol, 1988).
- ²F. Gabel, D. Bicout, U. Lehnert, M. Tehei, M. Weik, and G. Zaccai, *Q. Rev. Biophys.* **35**, 327 (2002).

- ³J. Smith, M. Krishnan, L. Petridis, and N. Smolin, "Integration of neutron scattering with computer simulation to study the structure and dynamics of biological systems," in *Dynamics of Biological Macromolecules by Neutron Scattering* (Bentham Publisher, 2011).
- ⁴A. Zen, V. Carnevale, A. Lesk, and C. Micheletti, *Protein Sci.* **17**, 918 (2008).
- ⁵E. Balog, D. Perahia, J. C. Smith, and F. Merzel, *J. Phys. Chem. B* **115**, 6811 (2011).
- ⁶M. Trapp, M. Trovaslet, F. Nachon, M. M. Koza, L. van Eijck, F. Hill, M. Weik, P. Masson, M. Tehei, and J. Peters, *J. Phys. Chem. B* **116**, 14744 (2012).
- ⁷M. Trapp, M. Tehei, M. Trovaslet, F. Nachon, N. Martinez, M. M. Koza, M. Weik, P. Masson, and J. Peters, *J. R. Soc., Interface* **11**, 20140372 (2014).
- ⁸J. Peters, N. Martinez, M. Trovaslet, K. Scannapieco, M. M. Koza, P. Masson, and F. Nachon, *Phys. Chem. Chem. Phys.* **18**, 12992 (2016).
- ⁹L. Van Hove, *Phys. Rev.* **95**, 249 (1954).
- ¹⁰N. Alberding, R. H. Austin, S. S. Chan, L. Eisenstein, H. Frauenfelder, I. C. Gunsalus, and T. M. Nordlund, *J. Chem. Phys.* **65**, 4701 (1976).
- ¹¹*NIST Handbook of Mathematical Functions*, edited by F. W. J. Olver, D. W. Lozier, R. F. Boisvert, and C. W. Clark (Cambridge University Press, 2010).
- ¹²V. Calandrini, V. Hamon, K. Hinsen, P. Calligari, M. C. Bellissent-Funel, and G. R. Kneller, *Chem. Phys.* **345**, 289 (2008).
- ¹³P. Schofield, *Phys. Rev. Lett.* **4**, 239 (1960).
- ¹⁴G. R. Kneller, *Phys. Chem. Chem. Phys.* **7**, 2641 (2005).
- ¹⁵E. Balog, T. Becker, M. Oettl, R. Lechner, R. Daniel, J. Finney, and J. C. Smith, *Phys. Rev. Lett.* **93**, 028103 (2004).
- ¹⁶C. D. Andersson *et al.*, *J. Phys. Chem. B* **122**, 8516 (2018).
- ¹⁷R. Zwanzig, *Proc. Natl. Acad. Sci. U. S. A.* **85**, 2029 (1988).
- ¹⁸H. Frauenfelder, S. G. Sligar, and P. G. Wolynes, *Science* **254**, 1598 (1991).
- ¹⁹Wolfram Research, Inc., Mathematica, Version 11.1 Wolfram Research, Inc., Champaign, Illinois, USA, 2017.